Songklanakarin J. Sci. Technol.
34 (6), 645-651, Nov. - Dec. 2012

SJST SONGKLANAKARIN JOURNAL OF SCIENCE AND TECHNOLOGY
http://www.sjst.psu.ac.th

Original Article

RF phase shifter using MEMS switches on a tapered coplanar waveguide

Nataraj Boothalingam[1]* and Porkumaran Karantharaj[2]

[1] *Department of Electronics and Communication Engineering, Sri Ramakrishna Engineering College, Coimbatore, Tamil Nadu, India.*

[2] *Dr. Nalla. G. Palaniswami Institute of Technology (NGP), Coimbatore, Tamil Nadu, India.*

Received 20 April 2012; Accepted 26 September 2012

Abstract

This paper presents the analysis and design of tapered coplanar waveguide based RF phase shifter using MEMS switches for microwave and millimeter-wave applications. The equivalent circuit of the phase shifter has been analyzed with the capacitances of MEMS switches in both up and down states. A control voltage applied between the center conductor and the switch's membrane actuates it and pulls down the membrane, creating a slow-wave transmission line. The loading capacitance gets added up with the line capacitance, thus varying the characteristic impedance of the line. This change in impedance varies the phase velocity, thereby producing a phase shift. The use of tapered coplanar waveguide as an alternative to the conventional waveguide produces an increase in phase shift per unit length with a small increase in insertion loss. By accurate design of the taper sections, the losses can be reduced further.

Keywords: MMIC, MEMS, CPW, DMTL, quasi-TEM, phase shifter, switches

1. Introduction

In modern communication technology, the devices and antennas size used is to be reduced and integrated with common very-large-scale integration (VLSI) technology. Phase shifter, an important device in communication system, should have a low loss to reduce electromagnetic interference and less size to reduce power consumption. Phase shifters are widely used in phased array antennas for electronics beam steering (Garver, 1972). There can be analog or digital phase shifters. Analog phase shifters provide a continuous phase shift compared with a discrete phase shift for digital phase shifter. Analog phase shifter provides a very low insertion loss compared to digital phase shifter. Many monolithic microwave integrated circuit (MMIC) phase shifters are developed for low-cost microwave applications.

RF microelectromechanical systems (MEMS) technology has provided many solutions for novel components and system implementation (Norvell *et al.*, 1999; Rebeiz, 2003). Many limitations in conventional technology can be overcome by this technology, mainly at high frequency applications. Realization of reconfigurable components such as switches, filters, varactors and phase shifters with low insertion loss, low power consumption, lesser intermodulation products and high linearity are achievable using this technology. Phase shifters for phased-array radar application's performances are increased using MEMS technology over conventional phase shifters in terms of size and losses. With decrease in size to micro-scale, force, size and boundary conditions should be considered for the design of MEMS structures (Salekdeh *et al.*, 2012). In Micro/nano-scale fabrication techniques, any ideal boundary condition could not be applied and boundary support conditions are to be theoretically validated. The use of MEMS switches for the design of tunable filter for X-band was reported (Islam *et al.*, 2008). Frequency is tuned using MAM fixed-fixed shunt switches producing variable capacitances for the band pass filter. The loss obtained is less than 0.7 dB for X-band.

Phased arrays consist of multiple stationary radiating elements, which are fed by tunable phase control units for

* Corresponding author.
Email address: bnatarajpillai@gmail.com

beam steering (Mailloux, 1994, Parker and Zimmerman, 2002). Phased arrays have separate components consisting feed network, phase shifters and antennas. Hybrid connection of these components increases the system size and also introduces parasitic effects, packaging costs and losses. These effects can be eliminated by implementing these individual components on a single substrate, producing monolithic phased arrays, possible through MEMS technology (Van Caekenberghe *et al.*, 2006, Topalli *et al.*, 2006).

This paper presents analysis of coplanar waveguide (CPW) and tapered CPW for the use in phase shifter design using RF MEMS technology. The phase shifter in this study is designed to operate at 20 GHz and employs analog distributed MEMS transmission line (DMTL) phase shifters. The phase shifters presented in this study are used to obtain an increase in phase shift per unit length using various types of CPW circuits.

2. Analysis of Coplanar Waveguide

High speed electronic devices used today can operate at frequencies beyond 100 GHz (Ho *et al.*, 1991; Ahmari *et al.,* 1996; Gill *et al.,* 1996). At these frequencies, for device connections and signal distribution, transmission lines are used to retain the signal fidelity. Among the various transmission lines, coplanar waveguides are preferred due to its integration capacity and fabrication compatibility with modern technologies. CPWs are important component for signal characterization and MMICs. The high impedance CPW transmission line and its equivalent circuit are shown in Figure. 1 a and b.

Wen (1969) proposed the first analytic formulas for calculating quasi-static wave parameters of CPW's using conformal mapping, based on the assumption that the substrate thickness is infinitely large and the ground wires of the CPW's are infinitely wide. Veyres and Fouad Hanna (1969) extended the application of conformal mapping t o CPW's with finite dimensions and substrate thicknesses. Fouad Hanna (1980) also has derived analytic formulas for CPS's on substrates with finite thicknesses. Results have a good accuracy only if the thicknesses of substrates are larger than the line dimensions, but diverge otherwise. To solve this problem, Ghione *et al.* (1984) have obtained more generalized formulas using the duality principle that the phase velocities of complementary lines are equal.

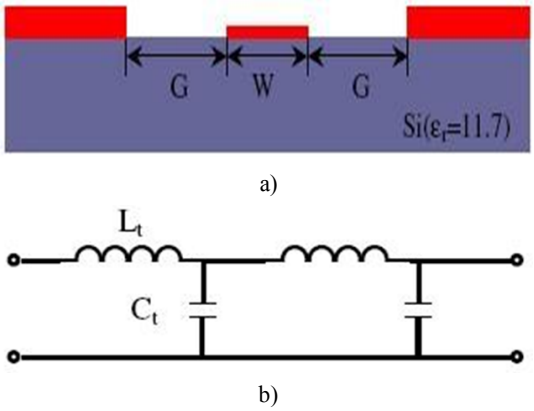

Figure 1. a) Layout of the CPW b) Equivalent circuit of the CPW

The conformal mapping is applied to obtain the characteristics of CPW transmission lines using the assumption that the propagation mode in the transmission lines is quasistatic, i.e., it is a pure TEM mode. The effective dielectric constant, phase velocity, and characteristic impedance, of a transmission line are given as (Gupta, 1979):

$$\varepsilon_{eff} = \frac{C_{CPW}}{C_0} \tag{1}$$

$$v_{ph} = \frac{c}{\sqrt{\varepsilon_{eff}}} \tag{2}$$

$$Z_0 = \frac{1}{C_{CPW} v_{ph}} \tag{3}$$

where C_{CPW} is the line capacitance of the CPW transmission line, C_0 is the line capacitance of the transmission line when no dielectrics exist, and c is the speed of light in free space. To obtain the quasi-static wave parameters of a transmission line, the capacitances C_{CPW} and C_0 -is to be found.

The Veyres – Fouad Hanna (1969) approximation (superposition of partial capacitances) is used, in which the line capacitance of the CPW is the sum of two line capacitances, i.e.,

$$C_{CPW} = C_0 + C_1 \tag{4}$$

$$C_0 = 4\varepsilon_0 \frac{K'(k)}{K(k)} \tag{5}$$

where K is the complete elliptical integral of the first kind, and K'(k) = K(k'). The variables k and k' are given as

$$k = \frac{x_c}{x_b}\sqrt{\frac{x_b^2 - x_a^2}{x_c^2 - x_a^2}} \tag{6}$$

$$k' = \sqrt{1 - k^2} \tag{7}$$

C_1 is the capacitance in which the electrical field exists only in a dielectric layer with thickness of h_1 and relative dielectric constant of e_{r1}-1.

$$C_1 = 2\varepsilon_0(\varepsilon_{r1} - 1)\frac{K'(k_1)}{K(k_1)} \tag{8}$$

where

$$k_1 = \frac{\sinh(\frac{\pi x_c}{2h_1})}{\sinh(\frac{\pi x_b}{2h_1})}\sqrt{\frac{\sinh^2(\frac{\pi x_b}{2h_1}) - \sinh^2(\frac{\pi x_a}{2h_1})}{\sinh^2(\frac{\pi x_c}{2h_1}) - \sinh^2(\frac{\pi x_a}{2h_1})}} \tag{9}$$

$$k_1' = \sqrt{1 - k_1^2} \tag{10}$$

The complete elliptical integrals of the first kind using the approximations given by Hilberg (1969) is given as

$$\frac{K(k)}{K'(k)} \approx \frac{2}{\pi}\ln\left(2\sqrt{\frac{1+k}{1-k}}\right) \quad \text{for} \quad 1 \le \frac{K}{K'} \le \infty \quad \text{and}$$

$$\frac{1}{\sqrt{2}} \le k \le 1 \qquad (11)$$

$$\frac{K(k)}{K'(k)} \approx \frac{\pi}{2\ln\left(2\sqrt{\frac{1+k'}{1-k'}}\right)} \quad \text{for} \quad 0 \le \frac{K}{K'} \le 1 \quad \text{and}$$

$$0 \le k \le \frac{1}{\sqrt{2}} \qquad (12)$$

3. Phase Shifter Design

The circuit design proposed here is based on a CPW DMTL whose phase velocity can be varied by using a single analog control voltage that varies the height of the MEMS loading capacitors, and the distributed capacitive loading on the transmission line and its propagation characteristics, as shown in Figure. 2a. This results in the analog control of the phase velocity and, therefore a true time delay phase shifter. The design requires a small value of loading capacitance per unit length, which results in very high actuation voltage. The topology of the CPW transmission line presented here, which varies the impedance, helps to increase the phase shift per unit length, resulting in a reduced physical line length, reduced pull down voltage and high capacitance ratio. The impedance and propagation velocity of the slow-wave transmission line are determined by the size of the MEMS bridges and their periodic spacing. The equivalent circuit of the loaded distributed MEMS transmission line is shown in Figure 2b. The shunt capacitance associated with the MEMS bridges is in parallel with the distributed capacitance of the transmission line, shown in Figure 2b.

From the analysis of CPW using conformal mapping, the per unit length capacitance is obtained. i.e. $C_t = C_{cpw}$. The unloaded lines per unit length capacitance and inductance are given by (Barker, 1998)

$$C_t = \frac{\sqrt{\varepsilon_{eff}}}{cZ_0} \quad \text{and} \quad L_t = C_t Z_0^2 \qquad (13)$$

where e_{eff} is the effective dielectric constant of the unloaded CPW transmission line, Z_0 is the characteristics impedance of the unloaded CPW line, and c is the free space velocity. The MEMS bridge only loads the transmission line with a parallel capacitance C_b, the loaded line impedance Z_l and phase velocity V_l of the loaded line, become

$$Z_l = \sqrt{\frac{L_t}{C_t + \frac{C_b}{s}}} \quad \text{and} \quad V_l = \frac{1}{\sqrt{L_t\left(C_t + \frac{C_b}{s}\right)}} \qquad (14)$$

where s is the periodic spacing of the MEMS bridges and C_b/s is the distributed MEMS capacitance on the loaded CPW line.

The MEMS bridge becomes unstable at $2g_0/3$, where g_0 is the zero-bias bridge height. The voltage at which this instability occurs is the "pull-down" voltage and is given by

$$V_p = \sqrt{\frac{8k}{27Ww} g_0^3} \ \text{V} \qquad (15)$$

The relative phase between the two states or the net phase shift ($\Delta\varphi$) is found from the change in the phase constant given by

$$\Delta\phi = \frac{\omega Z_0 \sqrt{\varepsilon_{eff}}}{c}\left(\frac{1}{Z_{lu}} - \frac{1}{Z_{ld}}\right) \qquad (16)$$

The design consists of a 7.94 mm long CPW transmission line whose centre conductor width (W) is 80 μm and the gap is 45 μm is fabricated on a 425 μm silicon substrate with a dielectric constant of 11.7 and tan(δ)=0.008 and with 11 shunt MEMS bridge capacitors placed periodically over the transmission line, shown in Figure 3. The height of the bridge above the centre conductor is 3 μm. The effective dielectric constant (ε_{eff}) of the unloaded CPW line has an average value of 6.25 and is linearly invariant with frequency. The width and span of the MEMS bridges are 40 μm and 340 ìm, respectively. The same parameters are used for designing

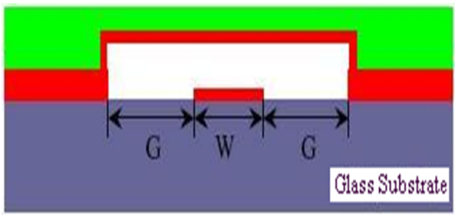

a)

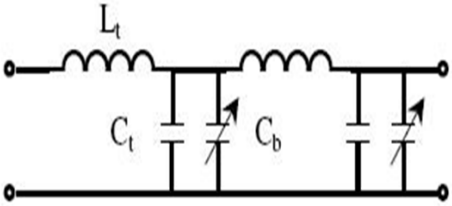

b)

Figure 2. a) Layout of the CPW with MEMS switch. b) Equivalent circuit of the CPW with MEMS switch.

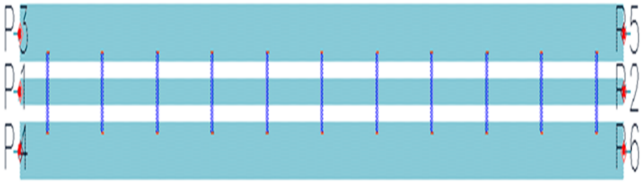

Figure 3. Layout of CPW loaded with 11 MEMS bridges.

MEMS phase shifter using tapered coplanar waveguide. By applying analog voltage, the MEMS switch is actuated from UP state to the DOWN state, which induces an increase in loading capacitance. The effect is an increase in total capacitance per unit length of the transmission line, and hence a change in phase velocity and characteristic impedance. The change in phase velocity produces a phase shift that is determined by the capacitance ratio C_{up}/C_{down} of the MEMS switch. The line has characteristic impedance of $Z_0 = 50\ \Omega$. If the bias voltage is applied directly between the membrane and the center conductor with a control circuit, the pull down voltage V_p can be reduced.

A section of two linear taper designs between two MEMS switches with spacing of 750 µm with varying impedances is shown in Figure 4. Table 1 shows the CPW width, gap and its impedance of the linear tapers used in the design. The characteristic impedances are calculated using quasi-TEM conformal mapping technique. The characteristic impedance of linear taper varies from 48 Ω to 78 Ω.

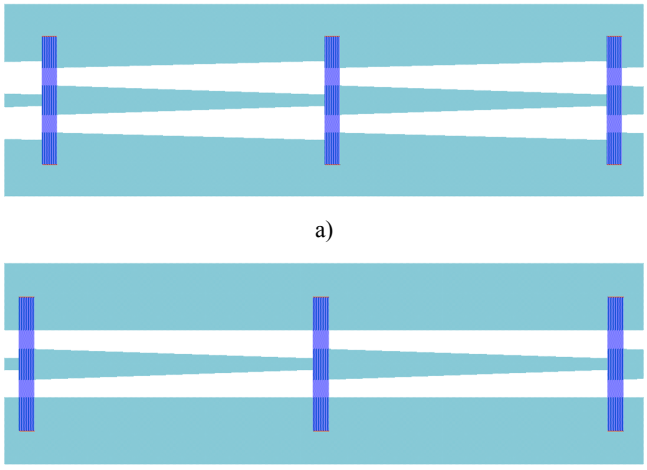

Figure 4. a) Layout of linear CPW Design-I between with 3 MEMS bridges. b) Layout of linear CPW Design-II between with 3 MEMS bridges.

4. Results

The simulated results are shown in Figure 5 to 7. The insertion loss of the phase shifter is -0.5 dB to -1.5 dB at 20 GHz and the phase shifter - Design II insertion loss is a little larger compared with the other two designs as its delay line is the longest. Both the output and input return loss is less in the range 5-10 dB. The change in phase shift is more in Design-I compared with conventional CPW and taper CPW design-II for the same length. Table 2 consolidates the results obtained for the various CPW phase shifter designs. From Table 2, the phase shift per unit length is more in taper Design-I compared with the other designs.

5. Conclusion

MEMS phase shifter using different transmission lines have been designed and simulated. It indicates tapered CPW

Table. 1. Calculated characteristic impedance for various widths and gaps.

Design – I			Design – II		
Width (µm)	Gap (µm)	Z_0 (Ω)	Width (µm)	Gap (µm)	Z_0 (Ω)
80	45	48.3	80	45	48.3
69	54	53.4	71	50	51.7
60	63	58.2	59	57	56.7
49	72	64.2	49	61	61.1
40	81	70.4	39	66	66.7
30	89	78.1	30	70	73.0

Table 2. Comparison of return loss, insertion loss, and phase shift of various CPW designs.

Parameters	Conventional CPW Phase shifter		Tapered CPW Phase Shifter – Design I		Tapered CPW Phase Shifter – Design II	
	UP State	DOWN State	UP State	DOWN State	UP State	DOWN State
S_{11} (dB)	-9.711	-7.941	-6.650	-8.168	-5.952	-5.533
S_{12} (dB)	-0.569	-0.804	-1.149	-0.854	-1.358	-1.224
S_{12} (°)	151	55	145	32	140	38
Change in Phase	96		113		102	

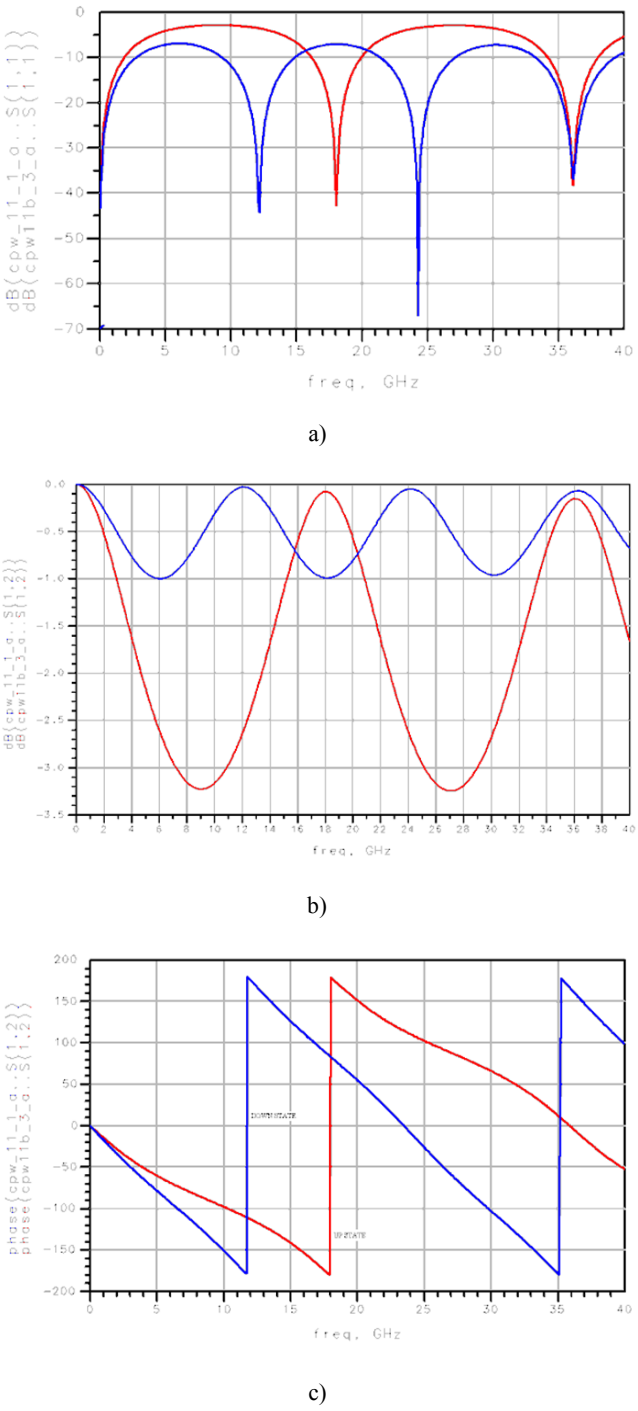

Figure 5. a) S_{11} (dB) of the conventional CPW in UP and DOWN state. b) S_{12} (dB) of the conventional CPW in UP and DOWN state. c) S_{12} (phase) of the conventional CPW in UP and DOWN state.

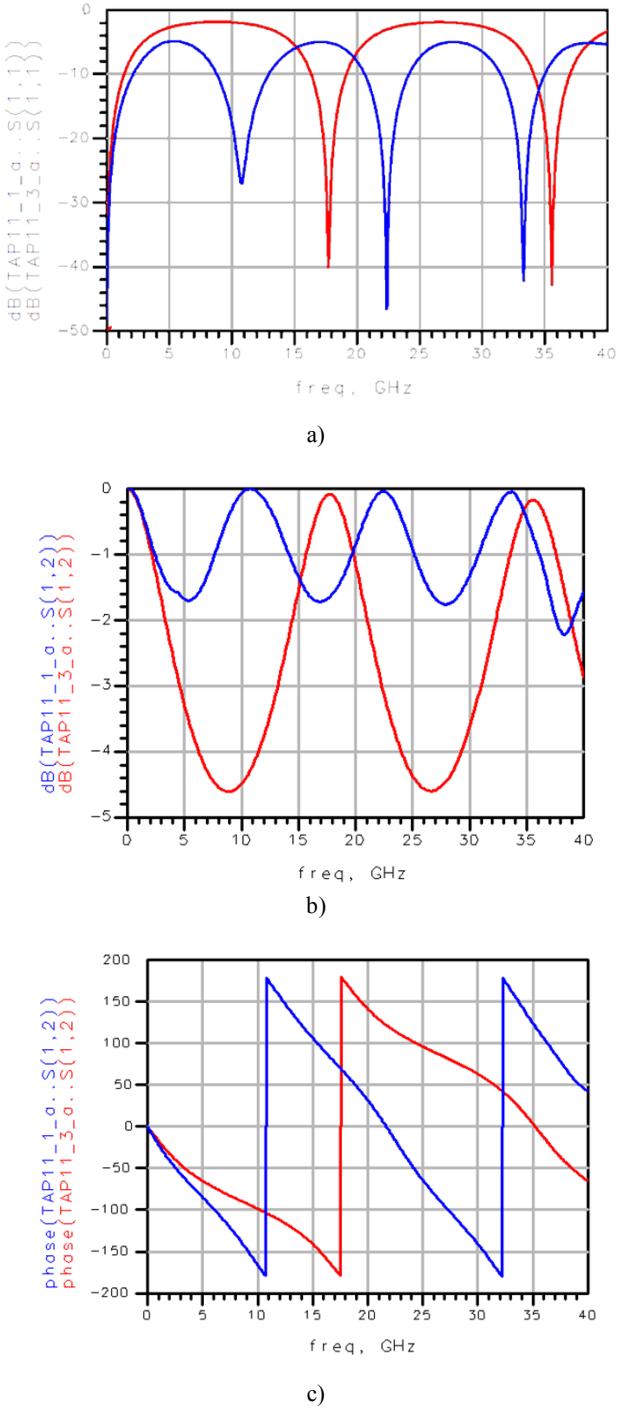

Figure 6. a) S_{11} (dB) of the linear tapered CPW Design – I in UP and DOWN state. b) S_{12} (dB) of the linear tapered CPW Design – I in UP and DOWN state. c) S_{12} (phase) of the linear tapered CPW Design – I in UP and DOWN state.

Design-I produce more phase shift among the three designs. Accurate phase shift change and relatively low insertion loss are obtained. The future work is to increase the isolation, reduce the insertion loss and mainly to increase the phase shift per unit length.

References

Ahmari, D. A., Fresina, M. T., Hartmann, Q. J., Barlage, D. W., Mares, P. J., Feng, M. and Stillman, G. E., 1996. High-speed InGaP/GaAs HBT's with a strained InxGa1 | |

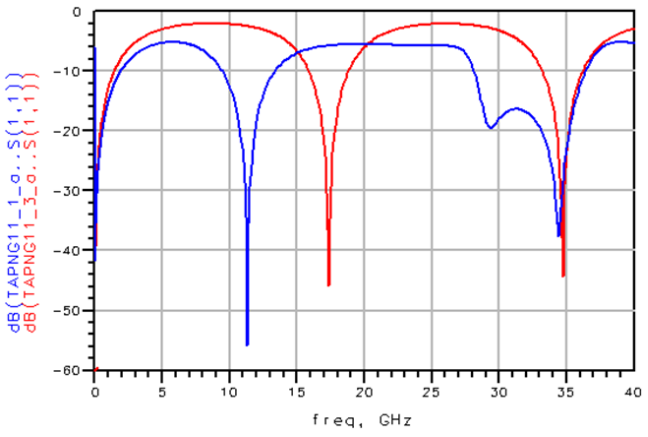

a)

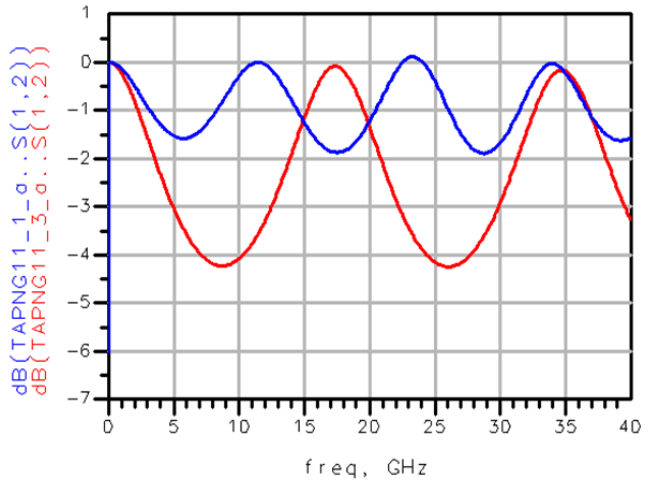

b)

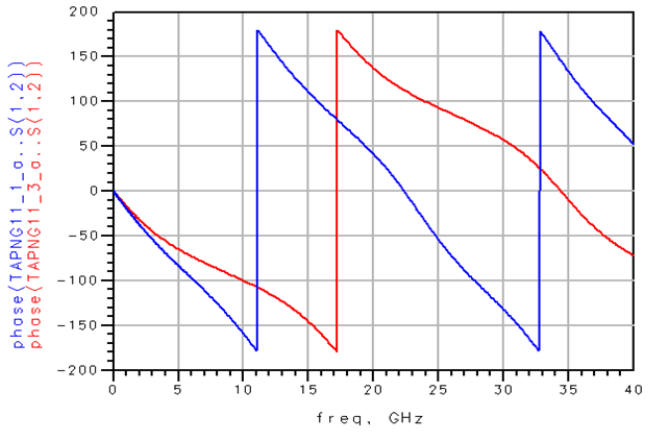

c)

Figure 7. a) S_{11} (dB) of the linear tapered CPW Design – II in UP and DOWN state. b) S_{12} (dB) of the linear tapered CPW Design – II in UP and DOWN state. c) S_{12} (phase) of the linear tapered CPW Design – II in UP and DOWN state

xAs base. Institute of Electrical and Electronics Engineers (IEEE) Electron Device Letters, 17, 226–228.

Barker, N. S. and Rebeiz, G. M., 1998. Distributed MEMS true-time delay phase shifters and wide band switches. Institute of Electrical and Electronics Engineers (IEEE) Transactions on Microwave Theory and Techniques, 46, 1881–1889.

Fouad Hanna, V. 1980. Finite boundary corrections to co-planar stripline analysis. Electronics Letters, 16, 604–606.

Garver, R.V. 1972. Broad-band diode Phase shifters. Institute of Electrical and Electronics Engineers (IEEE) Transactions on Microwave Theory and Techniques, 20, 314-323.

Ghione, G. and Naldi, C. 1984. Analytical formulas for co-planar lines in hybrid and monolithic MIC's. Electronics Letters, 20, 179–181.

Gill, D. M., Kane, B. C., Svensson, P., Tu, D. W., Uppal, P. N. and Byer, N. E. 1996. High-performance 0.1μm InAlAs/InGaAs high electron mobility transistors on GaAs. Institute of Electrical and Electronics Engineers (IEEE) Electron Device Letters, 17, 328–330.

Gupta, K. C., Garg, R. and Bahl, I. J. 1979. Microstrip Lines and Slotlines. Norwood, MA: Artech House., pp. 1-61.

Hilberg, W. 1969. From approximations to exact relations for characteristic impedances. Institute of Electrical and Electronics Engineers (IEEE) Transactions on Microwave Theory and Techniques, 17, 259–265.

Ho, P., Kao, M. Y., Chao, P. C., Duh, K. H., Ballingall, J. M., Allen, S. T., Tessmer, A. J. and Smith, P. M. 1991. Extremely high gain 0.15 μm gate-length InAlAs/InGaAs/InP HEMT's. Electronics Letters, 27, 325–327.

Islam, M. F., Ali, M. A. M. and Majlis, B. Y. 2008. RF MEMS-Based Tunable Filter for X-band Applications. Journal of Applied Sciences, 8, 189-191.

Mailloux, R. J. 1994. Phased Array Antenna Handbook. Norwood, MA: Artech House., pp. 20-35.

Norvell, B.R., Hancock, R. J., Smith, J. K., Pugh, M. I., Theis, S. W., and Kviakofsky, J. 1999. MEMS Technology applied to electronically scanned arrays for space based radar., Institute of Electrical and Electronics Engineers (IEEE) Proceedings of Aerospace Conference, Snowmass at Aspen, Colorado, United State, March 6-13, 1999, 239-247.

Parker, D. and Zimmerman, D.C., 2002. Phased Arrays – Part II: Implementations, applications, and future trends. Institute of Electrical and Electronics Engineers (IEEE) Transactions on Microwave Theory and Techniques, 50, 688-698.

Rebeiz, G.M. 2003. RF MEMS Theory, Design and Technology. Hoboken, NJ: Wiley., pp. 18-25.

Salekdeh, A. Y., Koochi, A., Beni, Y. T. and Abadyan, M. 2012. Modeling effects of three nano-scale Physical Phenomena on instability voltage of Multilayer MEMS/NEMS: Material size dependency, van der Waals Force and Non-classic support Conditions,

Trends in Applied Sciences Research, 7, 1-17.

Topalli, K., Unlu, M., Civi, O.A., Demir, S., Koc, S. and Akin, T.,2006. A monolithic phased array using 3-bit DMTL RF MEMS phase shifters. Institute of Electrical and Electronics Engineers (IEEE) Proceedings of Antennas and Propagation Society International Symposium, Albuquerque, New Maxico, United State, July 9-14, 2006, 517-520.

Van Caekenberghe, K., Vaha-Heikkila, T., Rebeiz, G.M. and Sarabandi, K. 2006. Ka band MEMS TTD passive electronically scanned phased array (ESA). Institute of Electrical and Electronics Engineers (IEEE) Proceeding of Antennas and Propagation Society International Symposium, Albuquerque, New Maxico, United State, July 9-14, 2006, 513-516.

Veyres, C., and Fouad Hanna, V., 1980. Extension of the application of conformal mapping techniques to coplanar lines with finite dimensions. International Journal of Electronics, 48, 47–56.

Wen, C. P. 1969. Coplanar waveguide: A surface strip transmission line suitable for nonreciprocal gyromagnetic device applications. Institute of Electrical and Electronics Engineers (IEEE) Transactions on Microwave Theory and Techniques, 17, 1087–1090.